Journal of Applied Electrochemistry **31**: 213–222, 2001.

The effects of 20 kHz and 500 kHz ultrasound on the corrosion of zinc precoated steels in $[Cl^-]$ $[SO_4^{2-}]$ $[HCO_3^-]$ $[H_2O_2]$ electrolytes

V. LIGIER, J.Y. HIHN*, M. WÉRY and M. TACHEZ
Laboratoire de Corrosion et de Traitements de Surface, Équipe de l'IUT, 30, Avenue de l'Observatoire, BP 1559, 25009 Besançon Cedex, France
*(*author for correspondence, e-mail: jean-yves.hihn@univ.Fwonte.Fr, tel.: +33(0)381 66 6892, fax: +33(0)381 66 6858)*

Received 18 December 1998; accepted in revised form 22 August 2000

Key words: power ultrasound, precoated steels, zinc corrosion test

Abstract

The effects of 20 and 500 kHz ultrasound on the corrosion of precoated steels were studied by analysing the behaviour of a zinc coated steel electrode in the corrosion electrolyte $[Cl^-]$ $[SO_4^{2-}]$ $[HCO_3^-]$ $[H_2O_2]$. The electrolyte was subjected to 20 kHz ultrasound, 500 kHz ultrasound and silent conditions. Zinc plated specimens were exposed to those solutions and growth of the corrosion products was studied by scanning electron microscopy, X-ray microanalysis and grazing incidence X-ray diffraction. Mass transfer measurements were taken on platinum macro- and microelectrodes; they highlighted a specific effect of ultrasound on the growth of zinc corrosion products depending on frequency. Ultrasound greatly influenced corrosion rates; however, the reaction sequence appeared unchanged by the use of an ultrasonic field compared to silent conditions.

1. Introduction

The corrosion resistance of new zinc coatings is commonly evaluated by long-term atmospheric exposure or by accelerated corrosion tests. A number of accelerated tests have been developed to give good rankings or lifetime predictions, but the results of accelerated and natural corrosion [1] still do not match. In previous work by the authors [2], the composition of new accelerated zinc corrosion electrolytes was derived from the chemistry of atmospheric pollutants. Zinc plated specimens were exposed to such solutions and the growth of the corrosion products was studied by scanning electron microscopy (SEM), energy dispersive X-ray analysis (EDS) and grazing incidence X-ray diffraction (GIXD). The main atmospheric zinc end-products were identified according to different natural environments: $NaZn_4Cl(OH)_6SO_4 \cdot 6\ H_2O$ for a marine atmosphere [3], $Zn_4SO_4(OH)_6 \cdot nH_2O$ for a rural environment [4], and $Zn_4Cl_2(OH)_4SO_4 \cdot 5\ H_2O$ in industrial and urban atmospheres [5]. These corrosion products grow, respectively, in $NaCl/Na_2SO_4/NaHCO_3/H_2O_2$, $Na_2SO_4/NaHCO_3/H_2O_2$ and $KCl/K_2SO_4/KHCO_3/H_2O_2$. Corrosion sequences have been established for these three electrolytes capable of reproducing mechanisms similar to the atmospheric corrosion sequences of zinc when exposed to marine, rural, and urban and industrial atmospheres. Accelerated corrosion tests performed in such electrolytes give satisfactory results as far as the nature of the zinc corrosion end-products and the corrosion sequences involved are concerned.

The zinc end-products grow in fissures generated on the zinc surface and then cover the whole zinc surface [2]. Work by Odnevall and Leygraf on atmospheric zinc corrosion shows that atmospheric zinc corrosion end-products grow on the zinc surface without any fissures [3–5]. Atmospheric metal corrosion can be considered as the result of chemical action by atmospheric pollutants and the more physical action of surface erosion by natural precipitation. This mechanical action must be added to the abrasive action of solid particles hitting the metal surfaces due to wind action. When dealing with electrolytes, an important way of inducing mechanical and even chemical changes is the use of an ultrasound source. Ultrasound has the most striking effect on heterogeneous reaction systems, particularly with a solid–liquid interface. The major influences of ultrasound upon electrochemical systems are enhancement of mass transport at the electrodes [6], alteration of the surface properties of the electrode [7], and sonochemical generation of electroactive species [8, 9]. As far as the corrosion of metals is concerned, Schmidt et al. reported that ultrasound can remove protective coatings from iron in sulphuric acid [10]. Hence, this electrochemical phenomenon is also affected in various ways by the use of ultrasonic waves, as confirmed by more recent work [11–14]. In our work, two ultrasound frequencies were used: one was low, 20 kHz, a type of ultrasound

generally used to increase heterogeneous kinetics [9]; the other frequency higher, 500 kHz, producing less mechanical effect but inducing interesting chemical properties in the electrolyte being irradiated. Recent work has shown that production of hydrogen peroxide by recombination of hydroxyl radicals is possible in sonicated oxygen saturated water [15, 16]. The H_2O_2 formation rate constant is higher in the 200–500 kHz range than in experiments done at 20 kHz.

In our work, zinc plated specimens were exposed under silent, 20 kHz and 500 kHz ultrasound conditions in $NaCl/Na_2SO_4/NaHCO_3/H_2O_2$ and $KCl/K_2SO_4/KHCO_3/H_2O_2$ electrolytes. The corrosion sequence was established for both by SEM, EDS and GIXD. The rate of H_2O_2 production was studied at 500 kHz in a sodium salt electrolyte. Mass transfer enhancement was evaluated by voltammetry in ultrasound agitated potassium ferri-/ferrocyanide electrolytes. Finally, corrosion rates were estimated by electrochemical impedance spectroscopy as a function of H_2O_2 concentration in a $NaCl/Na_2SO_4/NaHCO_3/H_2O_2$ electrolyte.

2. Experimental method

2.1. *Ultrasound generation and power measurements*

For all the experiments carried out at 20 kHz, the ultrasound source was a probe (Sonics & Materials, Danbury, USA). A titanium horn (25 mm dia.) was used to transmit ultrasound to the electrolytes. The high frequency transducers used in this work were developed by the Laboratory of Molecular and Environmental Chemistry (University of Savoie, Chambéry, France). The circular transducers were composed of a piezoelectric ceramic fixed on a circular plate (56 mm) of stainless steel or glass. The multifrequency generator was supplied by Electronics Service (St. Alban Leysse, France).

2.2. *Validation of the plated steel sample holder*

The working electrode was a rotating one. Several sample holders were machined to enable use and easy change of plated steel disc specimens [2]. The use of a plated steel sample holder was validated by voltamperometric curves recorded at a platinum foil (1 cm^2), immersed in potassium ferri-/ferrocyanide (5×10^{-3} mol dm^{-3}) and sodium sulfate (0.5 mol dm^{-3}) at 20 °C. The counter electrode was a titanium grid and the reference electrode was a saturated sulfate electrode (SSE). Ultrasound damage to the reference electrode was avoided by intercalating a frit glass between the irradiated electrolyte and the reference electrode (Figure 1). The potentiodynamic voltamograms were recorded at a 10^{-3} V s^{-1} scan rate with a PGP201 potentiostat (Radiometer Analytical) and controlled by Voltamaster software. The currents measured on the cathodic and anodic plateaux exhibited linear dependence (Figure 2) as previously reported by Levich [17]. The diffusion coefficients of both electroactive species were calculated using the slope as follows:

$$D^{2/3} = \frac{bv^{1/6}}{0.62\,nFC} \tag{2}$$

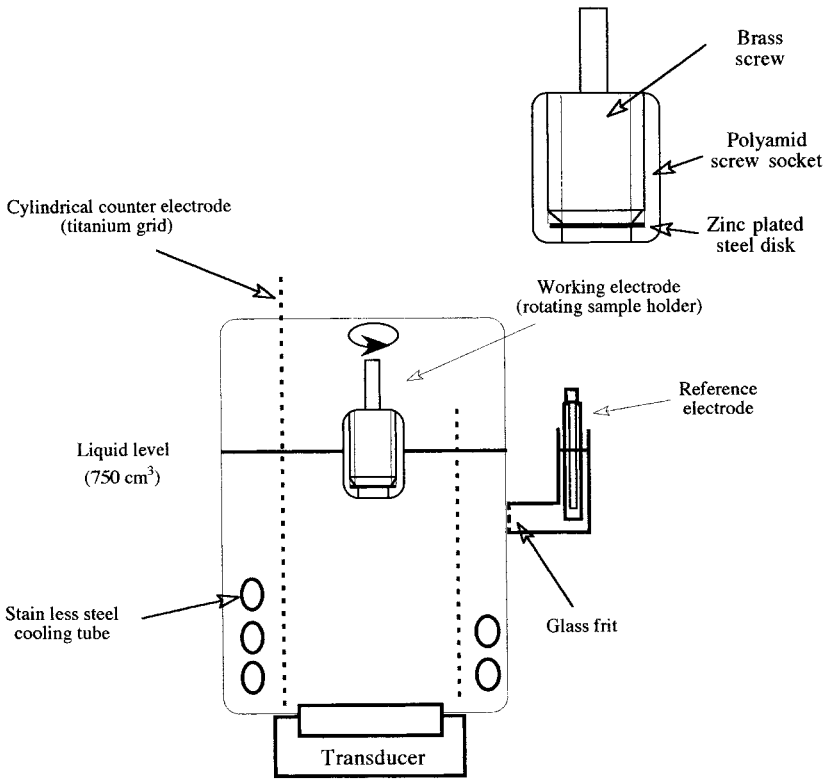

Fig. 1. Experimental apparatus used for the electrochemical measurements of zinc plated steel corrosion rates and mass transfer coefficients.

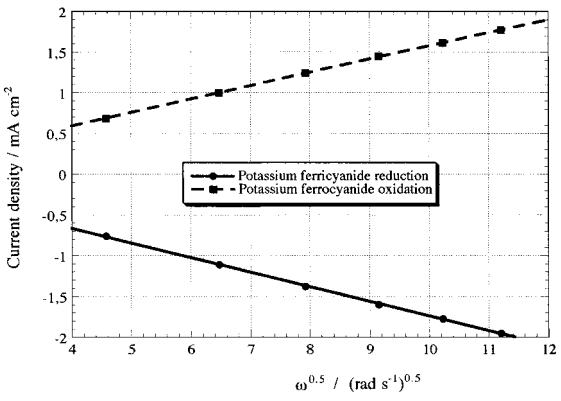

Fig. 2. Anodic and cathodic currents in potassium ferri-/ferrocyanide (5×10^{-3} mol dm^{-3}) at a plantinum electrode (1 cm^2) as a function of the electrode rotation rate.

where D is the diffusion coefficient (cm^2 s^{-1}), b is the absolute value of the slope (A cm^{-2} rad$^{1/2}$ s$^{-1/2}$), v is the kinematic viscosity of the fluid (cm^2 s^{-1}), n is the number of exchanged electrons, F is the faradaic constant (C) and C is the potassium ferri-/ferrocyanide concentration (mol cm^{-3}).

The following parameter values were used: $b_a = 0.164 \times 10^{-3}$ A cm^{-2} rad$^{1/2}$ s$^{-1/2}$, $b_c = 0.179 \times 10^{-3}$ A cm^{-2} rad$^{1/2}$ s$^{-1/2}$, $v = 10^{-2}$ cm^2 s^{-1}, $n = 1$, $F = 96\,500$ C, $A = 1$ cm^2 and $C = 5 \times 10^{-6}$ mol cm^{-3}.

The calculations gave diffusion coefficients of 4.07×10^{-6} cm^2 s^{-1} (Fe^{II}) and 4.64×10^{-6} cm^2 s^{-1} (Fe^{III}). These results matched the work by Benahcene et al. [18] on the effects of ultrasonically induced cavitation on electrochemical processes.

2.3. *Sample preparation*

Mild steel discs (3.14 cm^2) were used as test specimens. The alkaline zinc plating solution consisted of 130 g dm^{-3} NaOH and 17.4 g dm^{-3} ZnO. The additives were brighteners and surfactants supplied by Continental Parker Company. Each sample was plated for 30 min at 2 A dm^{-2}, corresponding to 11 μm zinc thickness due to bath efficiency; the part was then rinsed with deionized water, dried under hot air flow and stored in a dessicator.

2.4. *Exposure conditions*

Because the drying phase promoted the formation of a thin layer of hydrozincite $Zn_5(CO_3)_2(OH)_6$ on the coating surface, a small peak was visible on the diffractogram around $2\alpha = 13°$, suggesting the presence of zinc hydroxy carbonate on the noncorroded samples. So, the surface of the part was activated by dipping it into dilute HCl solution before rinsing it with deionized water and immersing it in the different electrolytes, that is, aqueous solutions of $NaCl/Na_2SO_4/NaHCO_3/H_2O_2$ and $KCl/K_2SO_4/KHCO_3/H_2O_2$ (Table 1). The efficiency of the activation phase was verified by the absence of the diffraction peak around $2\alpha = 13°$ on the diffractograms recorded on samples exposed for 30 s. A rotating disc electrode was used in the corrosion experiments and the electrochemical measurements to control the hydrodynamic conditions (500 rpm). The specimens were exposed for selected times then rinsed with deionized water and quickly dried under hot air flow.

2.5. *Analysis of the corrosion products*

As described previously [2], morphology and quantitative elemental analysis were performed using SEM and EDS. Crystalline phase determination was achieved by GIXD.

2.6. *Electrochemical measurements*

2.6.1. *Mass transfer evaluation*

I/E curves were recorded on platinum electrodes (quiescent or rotating) in potassium ferri-/ferrocyanide (5×10^{-3} mol dm^{-3}) and sodium sulfate (0.5 mol dm^{-3}) aqueous solutions. The quiescent platinum microelec-

Table 1. Composition of the accelerated corrosion electrolytes and immersion times of plated steel

NaCl /M	Na_2SO_4 /M	$NaHCO_3$ /M	H_2O_2 /M	Ultrasound /kHz	Immersion time /s, min or h
0.2	0.2	5×10^{-3}	1 and 4×10^{-3}	Switched off	30 s, 1 min, 3 min, 10 min, 30 min, 1 h, 3 h and 10 h
0.2	0.2	5×10^{-3}	1 and 4×10^{-3}	20 (35 W)	30 s, 1 min, 3 min, 10 min, 30 min, 1 h, 3 h and 10 h
0.2	0.2	5×10^{-3}	1 and 4×10^{-3}	500 (35 W)	30 s, 1 min, 3 min, 10 min, 30 min, 1 h, 3 h and 10 h
KCl /M	K_2SO_4 /M	$KHCO_3$ /M	H_2O_2 /M	Ultrasound /kHz	Immersion time /s, min or h
0.2	0.2	5×10^{-3}	1 and 4×10^{-3}	Switched off	30 s, 1 min, 3 min, 10 min, 30 min, 1 h, 3 h and 10 h
0.2	0.2	5×10^{-3}	1 and 4×10^{-3}	20 (35 W)	30 s, 1 min, 3 min, 10 min, 30 min, 1 h, 3 h and 10 h
0.2	0.2	5×10^{-3}	1 and 4×10^{-3}	500 (35 W)	30 s, 1 min, 3 min, 10 min, 30 min, 1 h, 3 h and 10 h

trode (0.009 cm^2) was prepared by heat-sealing Pt microwire (0.1 cm dia.) inside glass tubing. The electrode was then polished until a mirror like surface was achieved and its diameter was evaluated by optical microscopy (×1000) since the axis of the wire was not parallel to the glass tubing axis. The rotating disc electrode (500 rpm) was fitted with the plated steel sample holder, on which a platinum disc (2 cm dia.) stamped from a thin platinum foil was mounted.

2.6.2. *Electrochemical impedance spectroscopy*
The experiments were performed on the corrosion electrolyte $NaCl/Na_2SO_4/NaHCO_3/H_2O_2$. A.c. impedance measurements were taken using a 398 electrochemical impedance system (EG&G) in a frequency range of 10 kHz to 100 mHz with five points per decade. All measurements were carried out at the corrosion potential superimposing a 5 mV amplitude perturbing signal. Impedance diagrams were recorded after two hours of immersion time, switching off the ultrasonic agitation since the relationship between electrochemical impedance results and atomic absorption spectroscopy corrosion rates was established under silent conditions [2].

2.6.3. *Corrosion potentials as functions of the immersion time*
The samples were immersed and the open circuit potentials were measured against a saturated calomel electrode and recorded until the potentiometric transition from zinc to steel was achieved, that is, the appearance of a corroded substrate. Under ultrasonic conditions, the corrosion potential was recorded manually after switching off the ultrasonic irradiation and under silent conditions: $E_{corr} = f(t_{imm})$ record was operated by the software controlled potentiostat described in the steel sample holder validation section.

3. Results and discussion

To characterize the experimental ultrasonic conditions used in the corrosion experiments and to compare the results with those in the literature, the acoustic power transmitted to the electrolyte was measured by the calorimetric method developed by Mason et al. [19]. The rate of H_2O_2 formation was studied as per Pétrier et al. [15] and the mass transfer at the platinum electrodes was evaluated by electrochemical measurements with the ferri-/ferrocyanide system using the method of Trabelsi et al. [20]. The corrosion products were characterized by SEM, EDS and GIXD, and the corrosion rates of plated steel were estimated by electrochemical impedance spectroscopy as a function of the H_2O_2 concentration in a $NaCl/Na_2SO_4/NaHCO_3/H_2O_2$ electrolyte.

3.1. *Acoustic transmitted power measurements*

Both the 20 and the 500 kHz devices were tuned to obtain an acoustically transmitted power of 35 W, the maximum that could be achieved for long experiments by the high frequency apparatus fitted with a circular glass plate.

3.2. *Rate of H_2O_2 production in the corrosion electrolytes*

Hydrogen peroxide and sodium hydrogenocarbonate have predominant influences by, respectively, accelerating and diminishing the corrosion rate of zinc [2]. Pétrier et al. have given evidence that ultrasonic agitation of an aqueous oxygen saturated solution induces production of H_2O_2 by recombination of hydroxyl radicals. The reaction rate was enhanced when a high frequency (514 kHz) was used in comparison with the more commonly used low frequency (20 kHz) [15].

Therefore, a set of experiments was carried out to investigate the rate of H_2O_2 production in the corrosion electrolytes. 500 kHz was chosen as it is a value frequently used in the high frequency domain, providing significant H_2O_2 production. 750 ml of deionized water was used and oxygen was bubbled through the irradiated electrolyte. Sodium salts of the different anions contained in the corrosion electrolytes were added separately, in combinations of two or all together, to the deionized water (Table 2). The H_2O_2 concentration was determined by a colorimetric method described by Korman et al. [21]. The H_2O_2 concentration varies linearly (Figure 3) with irradiation time and the rate constants lie between 1.5 and 2.8×10^{-6} mol dm^{-3} min^{-1}. These values agree with the work by Pétrier et al. [16]. Moreover, the presence of sulfate ions seems to favour H_2O_2 production. Nevertheless, the expected concentrations remain negligible when compared with the quantity used in the corrosion electrolytes, typically 10^{-3} mol dm^{-3}.

3.3. *Estimation of mass transfer by an electrochemical method*

The mass transfer rates at electrodes can be greatly affected by ultrasound [6, 18, 20, 22]. From the diffusion current (I_L) recorded at a platinum electrode (surface S, radius r) immersed in potassium ferri-/ferrocyanide (concentration C, diffusion coefficient D), it is possible to calculate the mass transfer coefficient:

$$k_d = \frac{I_L}{FCS} \tag{3}$$

Table 2. Composition of the electrolytes for the study of H_2O_2 production under 500 kHz conditions

	NaCl /M	Na_2SO_4 /M	$NaHCO_3$ /M	H_2O_2 rate constants /10^6 mol dm^{-3} min^{-1}
A	0.2			1.4
B		0.2		1.9
C			5×10^{-3}	1.3
D	0.2		5×10^{-3}	1.5
E		0.2	5×10^{-3}	2
F	0.2	0.2		2
G	0.2	0.2	5×10^{-3}	1.5

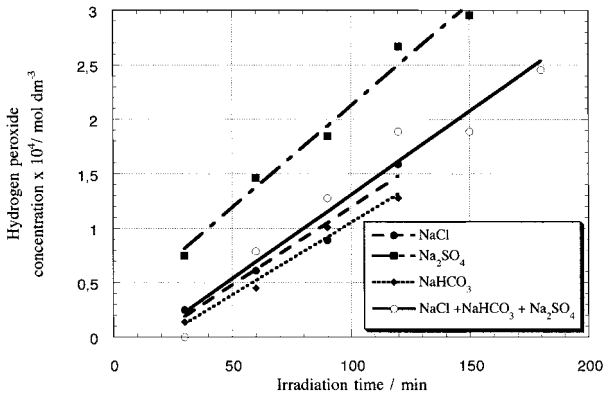

Fig. 3. Formation of hydrogen peroxide as a function of the 500 kHz irradiation time in the corrosion electrolytes.

so that the Sherwood number can be calculated, independently of electrolyte type and electrode geometry:

$$Sh = \frac{k_d r}{D} \tag{4}$$

There is some disagreement between authors about the choice of diameter or radius for the geometrical length in the Sherwood calculation. Work done in our laboratory with different electrode diameters led us to choose the radius r. Anodic and cathodic currents were obtained from I/E curves at platinum electrodes (quiescent or rotating) immersed in a potassium ferri-/ferrocyanide sodium sulfate electrolyte, with or without ultrasound. Table 3 presents the k_d and Sh values calculated from the resulting diffusion convection plateau, compared with values from the literature [18, 20, 22].

3.3.1. *Quiescent microelectrode measurements*

To compare local mass transfer to that achieved in previous studies, a 1 mm diameter platinum microelectrode was used first (Table 3). The Sherwood number of 110 obtained at 20 kHz is comparable to that found by Trabelsi et al. [20] at the same frequency. But at 500 kHz, the Sherwood number of 265 is higher than the results they obtained (40 to 110) at 561 kHz [20]. The difference may be partly explained by changes in operating conditions, 20 W transmitted power instead of 35 W, and different spatial location of the microelectrode [20, 22]. The importance of spatial location is confirmed by comparison with the results of Benhacène et al. [18], who found higher values at 20 and 500 kHz (Table 3). They found the maximum mass transfer efficiency near the transducer at 20 kHz instead of close to the liquid–gas interface at 500 kHz. In our work, corrosion tests were carried out at the same electrode/transducer distance for both frequencies, i.e. near the gas–liquid interface, which can favour a high Sherwood number at 500 kHz.

3.3.2. *Rotating macro electrode measurements*

The results with the microelectrodes showed that mass transfer conditions can vary due to many experimental conditions (frequency, power transmitted, electrode area and cell geometry, etc.). To characterize our accelerated corrosion test, mass transfer measurements were taken under the same experimental conditions, using electrode areas up to 3.14 cm^2 (2 cm dia.) and an electrode–transducer distance of 12.5 cm. The resulting I/E curves are shown in Figure 4. They have a characteristic shape in exhibiting oscillation in the signal, especially at 20 kHz. Nevertheless, these fluctuations are not as great as those observed when microelectrodes are used, in our work or in the literature [6, 23]. Only when small electrode areas are used can the time-dependent component be actually observed.

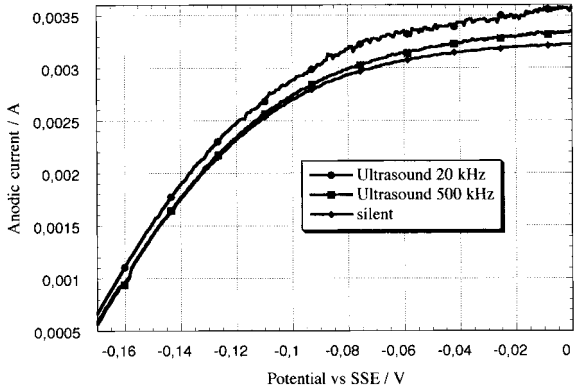

Fig. 4. Voltamperometric records in potassium ferri-/ferrocyanide (5×10^{-3} mol dm^{-3}) at a platinum rotating disc electrode (3.14 cm^2, 500 rpm) under silent, 20 and 500 kHz conditions.

Table 3. Sherwood numbers calculated at a platinum foil (3.14 cm^2) immersed in potassium ferri-/ferrocyanide for a 12.8 cm ultrasound source–working electrode (500 rpm) distance

Property	Microelectrodes		Microélectrodes		Microélectrodes		Macroelectrodes		
Authors	Benahcène et al. [18]		Trabelsi et al. [20, 22]		Present work				
	Quiescent electrode (QE)				QE		Rotating disc electrode		
Ultrasound frequency (kHz)	20	500	20	560	20	500	20	500	silent
Sherwood number	2110	980	110	40–110	110	265	283	267	519
$k_d \times 10^3$ (cm s^{-1})	68.9	31.5	19.8	7.2–19.8	10.2	24.6	1.31	1.24	1.20
$i_{lim} \times 10^3$ (A)	2.33	1.08	0.075	0.027–0.074	0.039	0.093	1.99	1.88	1.82
Transmitted power (W)	34	36	20	20	35	35	35	35	35
Working electrode	Glassy carbon		Pt	Pt	Pt	Pt	Pt	Pt	Pt

The Sherwood numbers are higher than those found with microelectrodes, and practically identical with or without ultrasound. The similar Sherwood numbers with ultrasound or in silent conditions suggest that the main contributor to convection is the rotation of the disc (500 rpm). Nevertheless, these values are the result of average mass transfer measurements and could be caused by violent local jet impingements. One only has to compare the corrosion products' morphology with and without ultrasound (Figure 5(a) and (b)).

Under silent conditions, the corrosion products are localised following logarithmic spirals (Figure 5(a)). These characteristic features are frequently observed on rotating disc electrode surfaces when obstacles like bubbles [24] or corrosion products are attached to the disc surface. The fluid flow is modified in the drag of the obstacle and mass transport is enhanced towards the electrode surface. At 500 kHz, the corrosion products are localized following concentric circles (Figure 5(b)) but the spirals inherent to the rotation of the disc are still visible. Lowering the frequency to 20 kHz seems to reduce these characteristic features. This result can be attained by very violent jet impingements, which can compensate each another in the average mass transfer measurements.

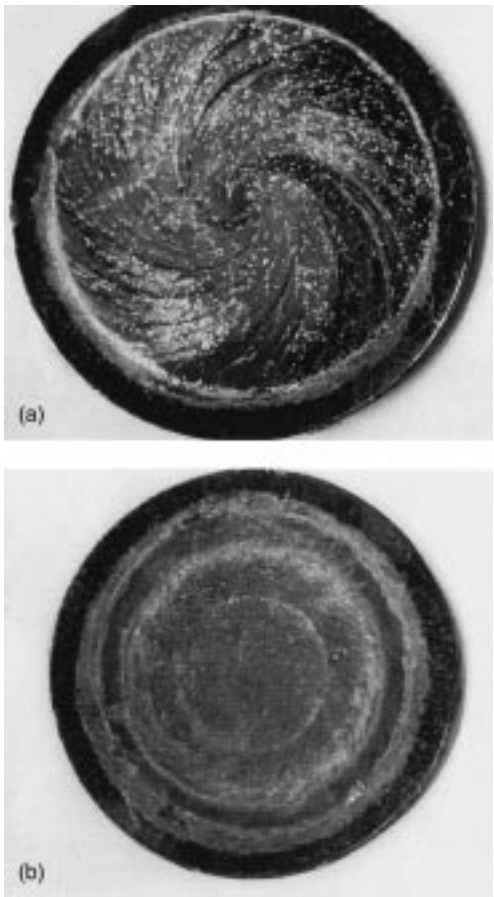

Fig. 5. Photographs of corrosion products on plated steel immersed in $NaCl/Na_2SO_4/NaHCO_3/H_2O_2$ (10^{-3} mol dm^3) after 1 h under silent conditions (a) or 500 kHz conditions (b).

3.4. *Growth of plated steel corrosion products in $NaCl/Na_2SO_4/NaHCO_3/H_2O_2$ and $KCl/K_2SO_4/KHCO_3/H_2O_2$ under silent, 20 or 500 kHz conditions*

Zinc plated steel discs were immersed for increasing immersion times and the growth of the corrosion products was studied by SEM, EDS and GIXD. Unless otherwise specified, the H_2O_2 concentration was 10^{-3} mol dm^{-3}.

3.4.1. *Silent conditions*

SEM/EDS analysis revealed the presence of small islands of corrosion products (max. 30 μm) on zinc plated steel discs immersed in $NaCl/Na_2SO_4/NaHCO_3/H_2O_2$ and $KCl/K_2SO_4/KHCO_3/H_2O_2$ electrolytes. After 30 s without ultrasound in $NaCl/Na_2SO_4/NaHCO_3/H_2O_2$ (Figure 6(a)), filaments of zinc oxide grow from these islands and their length can reach a few tens of micrometres. After three minutes of silent conditions in $KCl/K_2SO_4/KHCO_3/H_2O_2$, small grey areas are visible on the zinc surface. EDS analysis shows they are composed of zinc and oxygen but also carbon and traces of sulfur. After one hour of immersion in $NaCl/Na_2SO_4/NaHCO_3/H_2O_2$ under silent conditions, white compounds can be seen that always contain sulfur in the centre of these circular areas (Figure 6(b)). Fissures are visible around the grey zones measuring 30–40 μm. Chloride is detected in the cracks as well as zinc, oxygen, carbon and sulfur.

After immersion for 10 h in $NaCl/Na_2SO_4/NaHCO_3/H_2O_2$ in silent conditions, layered structures seem to grow in the centre of the circular grey zones (Figure 6(c)). Their composition corresponds to $NaZn_4ClSO_4(OH)_6 \cdot 6\,H_2O$ for a $NaCl/Na_2SO_4/NaHCO_3/H_2O_2$ electrolyte and $Zn_4Cl_2(OH)_4SO_4 \cdot 5\,H_2O$ for a $KCl/K_2SO_4/KHCO_3/H_2O_2$ electrolyte. After 40 h of immersion in $NaCl/Na_2SO_4/NaHCO_3/H_2O_2$, the peaks corresponding to these compounds are displayed on the X-ray diffractogram [2]. Those compounds have only recently been discovered; they belong to zinc chlorohydroxysulfate corrosion products [24]. $NaZn_4ClSO_4(OH)_6 \cdot 6\,H_2O$ grows in marine environments [3] and $Zn_4Cl_2(OH)_4SO_4 \cdot 5\,H_2O$ develops in urban and industrial environments [5].

3.4.2. *500 kHz ultrasound conditions*

In ultrasonic conditions, white islands of corrosion products are also detected in both electrolytes for low immersion time samples, but the filaments observed in the silent conditions are smaller (Figure 6(d) compared with Figure 6(a)).

After 30 min of ultrasonic irradiation, craters are visible in the centre of the disc, measuring up to 150 μm. Zinc and oxygen are also detected on their edges (Figure 6(e)).

After 1 h of immersion, large zones are covered by layered structures (Figure 6(f)) with a composition corresponding to that of $Zn_4Cl_2(OH)_4SO_4 \cdot 5\,H_2O$ for a

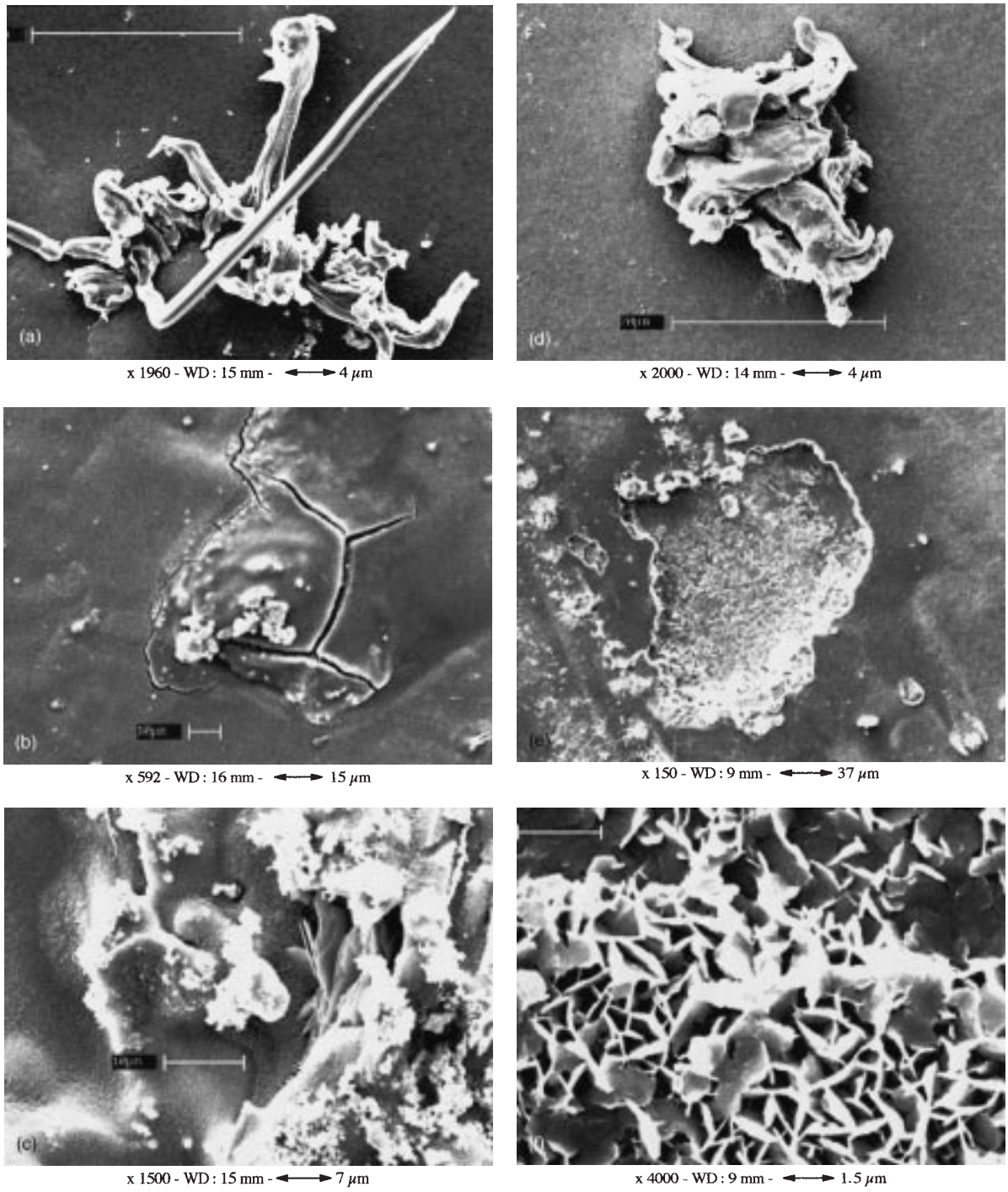

Fig. 6. Scanning electron micrographs of corrosion products on plated steel immersed in $NaCl/Na_2SO_4/NaHCO_3/H_2O_2$ (10^{-3} mol dm^3) after 30 s under silent conditions (a), $NaCl/Na_2SO_4/NaHCO_3/H_2O_2$ (10^{-3} mol dm^3) after 1 h under silent conditions (b), $NaCl/Na_2SO_4/NaHCO_3/H_2O_2$ (10^{-3} mol dm^3) after 10 h under silent conditions (c), $NaCl/Na_2SO_4/NaHCO_3/H_2O_2$ (10^{-3} mol dm^3) after 30 s under 500 kHz conditions (d), $NaCl/Na_2SO_4/NaHCO_3/H_2O_2$ (10^{-3} mol dm^3) after 30 min under 500 kHz conditions (e) and $NaCl/Na_2SO_4/NaHCO_3/H_2O_2$ (10^{-3} mol dm^3) after 1 h under 500 kHz conditions (f).

$KCl/K_2SO_4/KHCO_3/H_2O_2$ electrolyte and $NaZn_4ClSO_4(OH)_6 \cdot 6\ H_2O$ for a $NaCl/Na_2SO_4/NaHCO_3/H_2O_2$ electrolyte.

3.4.3. *20 kHz ultrasound conditions*

Under 20 kHz ultrasonic conditions, white islands of corrosion products are also detected on the low immersion time samples in both electrolytes, but their shapes have changed compared with the 500 kHz corrosion islands.

After 1 h of immersion in $KCl/K_2SO_4/KHCO_3/H_2O_2$, layered structures cover very large zones. The composition corresponds to that of $Zn_4Cl_2(OH)_4SO_4 \cdot 5\ H_2O$ for a $KCl/K_2SO_4/KHCO_3/H_2O_2$ electrolyte and $NaZn_4ClSO_4(OH)_6 \cdot 6\ H_2O$ for a $NaCl/Na_2SO_4/NaHCO_3/H_2O_2$ electrolyte. When the H_2O_2 concentration is

increased to 4×10^{-3} mol dm^{-3}, less corrosion products are visible on the zinc surface, suggesting a decrease in the zinc plated steel corrosion rate. Most of the corrosion products formed on the zinc plated steel remain on its surface and are not directly solubilized in those electrolytes [25]. Ultrasound seem to prevent the growth of the filaments observed on silent condition samples, due to the erosive effects of the microjets generated by the implosion of the cavitation bubbles.

Ultrasound induces surface damage in the centre of the discs [11, 14]. These results are in accordance with the work reported by Trethewey et al. who found a synergistic effect of ultrasonically induced corrosion (20 kHz) on a Cu/Mn/Al alloy immersed in sea water [12]. The formation of cracks, as previously observed [12], can be explained by the fact that when ultrasonic waves are propagated through an electrolyte, the oscillations of the molecules induce the formation of regions of pressure oscillations. For a given value of relative depression, the forces holding the liquid together are overcome and cavitation bubbles containing dissolved gases and water vapour appear. The behaviour of the bubble depends on its size and on the nature of the local acoustic field, which determines whether it remains stable or not [26]. The behaviour of spherical bubbles collapsing in the vicinity of a solid wall has been studied theoretically [27, 28]. The presence of an adjacent solid wall results in the production of jets as the vapour bubble collapses. It is presumed that the jets play an important role in surface cavitation damage [27].

$NaZn_4ClSO_4(OH)_6 \cdot 6\,H_2O$ and $Zn_4Cl_2(OH)_4SO_4 \cdot 5\,H_2O$ grow in cracks generated on the zinc surface and then in the centre of the carbonated zones after 1 and 10 h in silent conditions, whereas large zones are covered by this compound after only one hour in the ultrasonic conditions with no fissure mentioned. Odnevall and Leygraf do not report the formation of any fissure in their studies [3–5, 29]. This accelerated growth is confirmed by X-ray diffraction measurements. There is evidence of zinc chlorosulphate presence after one hour of immersion time in ultrasonic conditions.

The use of ultrasound has a specific effect on the growth of the zinc corrosion products depending on the ultrasound frequency, whereas the reaction sequence seems to be identical in the different media, whether the electrolyte is irradiated or not. Ultrasound completes the resemblance between the morphology of the main atmospheric zinc end-products formation in [Cl^-] [SO_4^{2-}] [HCO_3^-] [H_2O_2] electrolytes [2] with natural exposures, i.e. no fissures mentioned [3–5, 29], by the activation of the zinc surface and the subsequent growth of the corrosion products straight on the metal surface.

3.5. *Estimation of the corrosion rates of plated steel in $NaCl/Na_2SO_4/NaHCO_3/H_2O_2$ under silent or ultrasound (20 and 500 kHz) conditions*

For zinc plated steel exposed to $NaCl/Na_2SO_4/NaHCO_3/H_2O_2$, polarisation curves were recorded in previous work [25] showing an anodic domain under charge transfer activation and a cathodic domain controlled by diffusion. In this case, the corrosion current and the charge transfer resistances are still linked together [30, 31]. Based on the theoretical link between the corrosion current and the charge transfer resistance R_t [31], a relationship was calculated by combining electrochemical measurements with the results of a direct corrosion evaluation method. Average corrosion current values i_{corr} were calculated by evaluating the total oxidized zinc concentration by means of atomic absorption spectroscopy after dissolution of the corrosion products [2]. From electrochemical impedance spectroscopy, it was possible to obtain $(1/R_t)$ proportional to a quasi-instantaneous corrosion rate. An integration was necessary, that is,

$$\frac{1}{t_{imm}} \int_0^t \frac{1}{R_t} dt$$

to compare average corrosion currents. A linear dependence was obtained [2], as it was accounted from the theoretical relation from Epelboin's work [31]. In this work, the corrosion current density is calculated from the extrapolation of the charge transfer resistances from impedance diagrams (Figure 7). The results are given as a function of the H_2O_2 concentration in Figure 8. Zinc electroplated steel discs are immersed in the corrosion electrolytes.

3.5.1. *Silent conditions*

At low H_2O_2 concentrations, a low corrosion rate is observed in the silent conditions. The corrosion current remains low before increasing at a 3×10^{-3} mol dm^{-3} H_2O_2 concentration (Figure 8). These results are confirmed by other electrochemical measurements. The corrosion potential of plated steel is recorded during the immersion of zinc in the same electrolytes, that is, $NaCl/Na_2SO_4/NaHCO_3$ /H_2O_2, in order to compare the

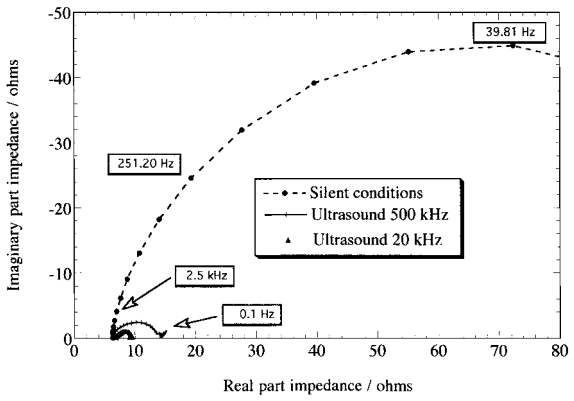

Fig. 7. Plot of impedance record obtained on plated steel after 2 h of immersion time of plated steel immersed in $NaCl/Na_2SO_4/NaHCO_3/H_2O_2$ (10^{-3} mol dm^{-3}) under silent (- - ● - -), 500 V (—|—) and 20 kHz (▲) conditions.

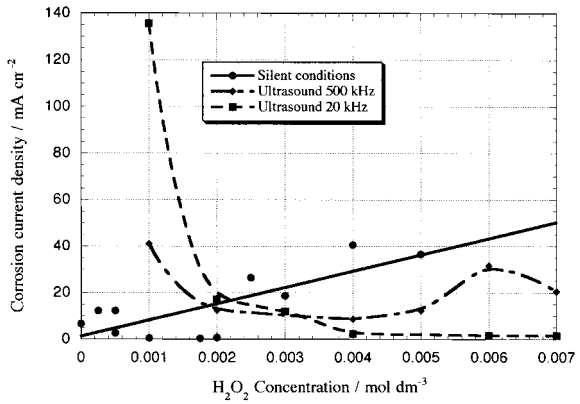

Fig. 8. Corrosion current densities at plated steel electrodes immersed in $NaCl/Na_2SO_4/NaHCO_3/H_2O_2$ under silent, 500 and 20 kHz conditions as a function of the H_2O_2 concentration.

protective capacity of the corrosion products developed in those media. At higher H_2O_2 concentrations (4×10^{-3} mol dm^{-3}), the situation is reversed (Figure 8) and the corrosion current density is the highest in the silent conditions. The $E_{corr} = f(t_{imm})$ measurements confirm this result and show that the transition of potential from zinc to steel is achieved and slightly superior to 1 hour of immersion (Figure 9).

3.5.2. *20 kHz conditions*

The chemical stability of hydrogen peroxide (around 10^{-3} mol dm^{-3}) was verified over time under 20 and 500 kHz ultrasonic fields [25]. At low H_2O_2 concentrations, the corrosion current is maximum under 20 kHz ultrasonic conditions. The corrosion current density is nearly four times higher than in the 500 kHz conditions for identical transmitted power and 200 times higher than in the silent conditions (Figure 8). Enhancement as high as a factor of 186 was reported in the case of weight loss measurements taken on NAB (nickel–aluminium–bronze) immersed in sea water under 20 kHz compared to silent conditions [14]. Whillock and Harvey found weaker factors for the corrosion of stainless steel in the nitric acid/chloride system. When the metal is corroding actively, sonication at a frequency of 55 kHz increases the corrosion rate by a factor between 3 and 6 [13]. Al-Hashem et al. [14] report greater enhancements of corrosion rates under ultrasound conditions. Using 20 kHz ultrasonic agitation, the corrosion current density decreases continuously to very low values as a function of the H_2O_2 concentration (Figure 8). The small corrosion current densities are compatible with those recorded by Whillock et al. on passivated stainless steel. The $E_{corr} = f(t_{imm})$ measurements confirm this result; the time corresponding to the transition potential from zinc to steel is not attained during the experimental time in the case of the smallest H_2O_2 concentration (Figure 10).

At higher H_2O_2 concentrations (e.g., 4×10^{-3} mol dm^{-3}), the lowest corrosion rate is observed in the 20 kHz conditions (Figure 8), as was previously predicted by the SEM photographs in Figure 6. The magnitude of the development of corrosion products may therefore be related to the weakness or the width of corrosion damage.

Since there is no need to give further evidence of the electrochemical nature of zinc corrosion in aqueous electrolytes containing sulfate or chloride ions [32], the uniformity of the zinc corrosion layer observed at high H_2O_2 concentration under 20 kHz ultrasound may partly impede the establishment of electrochemical cells. The corrosion phenomenon could therefore be slowed.

3.5.3. *500 kHz conditions*

At low H_2O_2 concentrations, 500 kHz ultrasound enhances the corrosion rate by a factor of 70 compared to silent conditions (Figure 8). Under 500 kHz conditions, the corrosion current values decrease as a function of the H_2O_2 concentration, stabilise near 5 mA cm^{-2} and rise again from 5×10^{-3} mol dm^{-3} (Figure 8). The $E_{corr} = f(t_{imm})$ measurements confirm this result; the time necessary to reach the transition potential from zinc to steel seems to be independent of the H_2O_2 concentration (Figure 10). The corrosion resistance of the plated steel discs is therefore different depending on the ultrasound frequency but that difference cannot be

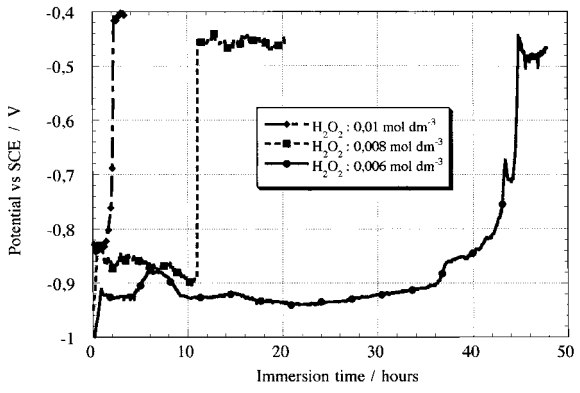

Fig. 9. Corrosion potential of plated steel immersed in $NaCl/Na_2SO_4/NaHCO_3/H_2O_2$ against immersion time under silent conditions.

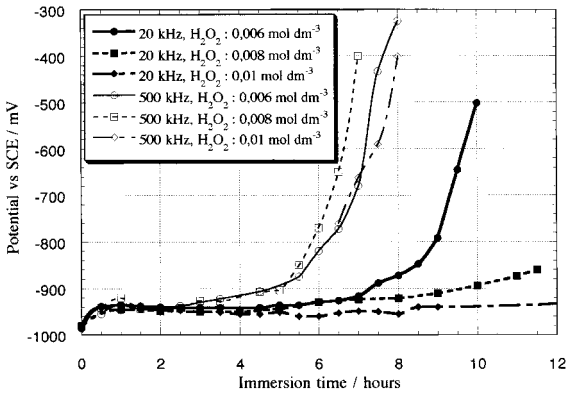

Fig. 10. Corrosion potential of plated steel immersed in $NaCl/Na_2SO_4/NaHCO_3/H_2O_2$ against immersion time under 20 and 500 kHz ultrasound.

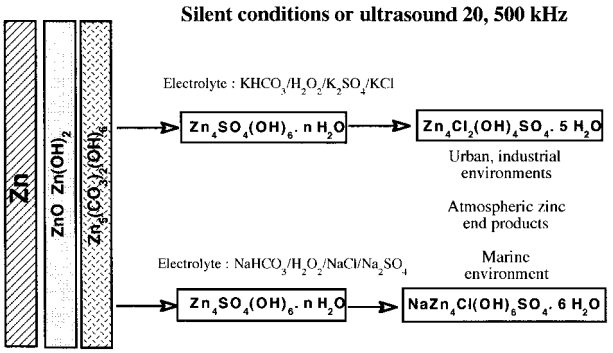

Fig. 11. Corrosion sequence of plated steel in $NaCl/Na_2SO_4/NaHCO_3/H_2O_2$ and $KCl/K_2SO_4/KHCO_3/H_2O_2$ electrolytes under 20 and 500 kHz ultrasound.

attributed to a major modification of global mass transfer since the Sherwood numbers are similar in silent and ultrasonic conditions (Table 3).

But both ultrasound frequencies increase or decrease the corrosion rate of zinc plated steel in $NaCl/Na_2SO_4/NaHCO_3/H_2O_2$ electrolytes. High hydrogen peroxide concentration and ultrasound decrease corrosion whereas low concentration and ultrasound increase corrosion. Less corrosion products are then observed on the zinc plated steel surface and the corrosion layer is more uniform.

4. Conclusion

The action of ultrasound on the corrosion of plated steel in $[Cl^-]$ $[SO_4^{2-}]$ $[HCO_3^-]$ $[H_2O_2]$ electrolytes does not modify the corrosion sequence but enhances the zinc reactivity (Figure 11). This phenomenon increases the zinc corrosion rates in $NaCl/Na_2SO_4/NaHCO_3/H_2O_2$ electrolytes at low H_2O_2 concentrations. Nevertheless, the situation is reversed when the H_2O_2 concentration is higher and the corrosion layer is more uniform. $[Cl^-]$ $[SO_4^{2-}]$ $[HCO_3^-]$ $[H_2O_2]$ electrolytes permit the formation of the natural zinc corrosion products observed in marine, urban and industrial atmospheres with corrosion sequences very close to natural exposure. Moreover, the chemical action of those electrolytes can be made up by the specific action of ultrasound on the zinc corrosion products' distribution. Hence, the design of a new accelerated zinc corrosion test could be considered in the future.

Acknowledgements

Acknowledgement is made to Pr. C. Pétrier for the loan of transducers and for technical discussions (LCME, Laboratoire de Chimie Moléculaire et Environmentale, Université de Savoie). We also gratefully acknowledge the LMIT (Laboratoire de Métrologie des Interfaces Techniques, Montbéliard Site) for grazing incidence diffraction measurements. We thank the CME (Centre de Microscopie Electronique, Besançon) and the LPMO (Laboratoire de Physique et Métrologie des Oscillateurs, Besançon,) for SEM/EDS analysis. We also wish to thank Novelect–EDF for their financial participation in this work.

References

1. C. Barreau and D. Massinon, *Proceedings of the Congress* 'Le zinc et l'anticorrosion: Essais et performances', St Ouen (1993).
2. V. Ligier, M. Wéry, J.Y. Hihn and M. Tachez, *Corros. Sci.* **41**(6) (1999) 1139–64.
3. I. Odnevall and C. Leygraf, *Corros. Sci.* **34**(8) (1993) 1213.
4. I. Odnevall and C. Leygraf, *Corros. Sci.* **36**(6) (1994) 1077.
5. I. Odnevall and C. Leygraf, *Corros. Sci.* **36**(9) (1994) 1551.
6. C.R.S. Hagan and L.A. Coury, *Anal. Chem.* **66**(3) (1994) 399.
7. R. Walker, *Chem. Brit.* (1990) 251.
8. J.P. Lorimer and T.J. Mason, *Chem. Soc. Rev.* **16** (1987) 239.
9. D.J. Walton and S.S. Phull, *Adv. Sonochem.* **4** (1996) 205–84.
10. G. Schmidt and L. Ehret, *Z. Electrochem.* **43** (1937) 408.
11. H.V. Fairbanks, *Internat. Congress on Metal–ICMC 9th Toronto* **4** (1984) 494.
12. K.R. Trethewey, T.J. Haley and C.C. Clark, *Br. Corros. J.* **23** (1988) 55.
13. G.O.H. Whillock and B.F. Harvey, *Ultrasonics Sonochem.* **3** (1996) 111.
14. A. Al-Ashem, P.G. Caceres, W.T. Riad and H.M. Shalaby, *Corros. Sci.* **51**(5) (1995) 331.
15. C. Pétrier, A. Jeunet, J.L. Luche and G. Reverdy, *J. Am. Chem. Soc.* **114** (1992) 3148.
16. C. Pétrier, M.F. Lamy, A. Francony, V. Renaudin, N. Gondrexon, B. David, A. Benhacène, *J. Phys. Chem.* **98** (1994) 10514.
17. V.G. Levich, 'Physicochemical Hydrodynamics' (Prentice Hall, Englewood Cliffs, NJ, 1962).
18. A. Benahcene, C. Pétrier and G. Reverdy, *New J. Chem.* **19** (1995) 989–95.
19. T.J. Mason, J.P. Lorimer and D.M. Bates, *Ultrasonics* **30**(1) (1992) 40.
20. F. Trabelsi, H.A. Lyazidi, J. Berlan, P.L. Fabre, H. Delmas and A.M. Wilhelm, *Ultrasonics Sonochem.* **3** (1996) S125.
21. C. Kormann, D.W. Bahnemann and M.R. Hoffmann, *Environ. Sci. Technol.* **22** (1988) 798.
22. F. Trabelsi, H. Aï-Lyazidi, B. Ratsimba, A-M. Wilhelm, H. Delmas, P-L. Fabre and J. Berlan, *Chem. Eng. Sci.* **51**(10) (1996) 1857–65.
23. E.L. Cooper and L.A. Coury, *J. Electrochem. Soc.* **145**(6) (1998) 1994.
24. O. Devos, A. Olivier, J.P. Chopart, O. Aaboubi and G. Maurin, *J. Electrochem. Soc.* **145**(1) (1998) 401.
25. V. Ligier, PhD Thesis, Besançon, University of Franche Comté (1997).
26. T.G. Leighton, *Ultrasonics Sonochem.* **2** (1995) 123.
27. A. Shima and K. Nakajima, *J. Fluid Mech.* **80** (1977) 369.
28. W. Lauterborn and H. Bolle, *J. Fluid Mech.* **72**(2) (1975) 391.
29. I. Odnevall and C. Leygraf, 'Atmospheric Corrosion', ASTM STP (1995) p. 1239.
30. M. Stern and A.L. Geary, *J. Electrochem. Soc.* **104**(1) (1957) 56.
31. I. Epelboin, C. Gabrielli, M. Keddam and H. Takenouti, '*in* F. Mansfeld and U. Bertocci (Eds), Electrochemical Corrosion Testing', ASTM STP 727 (1980).
32. U.R. Evans, 'An introduction to Metallic Corrosion' Vol. 2 (E. Arnold, London, 1981) p. 43.